Atmospheric Environment 242 (2020) 117672

Contents lists available at ScienceDirect

Atmospheric Environment

journal homepage: http://www.elsevier.com/locate/atmosenv

A modeling study of the regional representativeness of surface ozone variation at the WMO/GAW background stations in China

Ningwei Liu [a], Jianzhong Ma [b,*], Wanyun Xu [b], Yuhang Wang [c], Andrea Pozzer [d], Jos Lelieveld [d]

[a] Institute of Atmospheric Environment, China Meteorological Administration, Shenyang, Liaoning, 110016, China
[b] State Key Laboratory of Severe Weather & CMA Key Laboratory of Atmospheric Chemistry, Chinese Academy of Meteorological Sciences, Beijing, 100081, China
[c] Georgian Institute of Technology, Atlanta, GA, 30332-0340, USA
[d] Max Planck Institute for Chemistry, D-55020, Mainz, Germany

HIGHLIGHTS

- The EMAC model is evaluated against surface ozone measured at the WMO/GAW background stations in China.
- The contributions of ozone originating from various latitude bands simulated by EMAC are analyzed.
- Regional representativeness of surface ozone variation at the six Chinese WMO/ GAW stations is investigated.

ARTICLE INFO

Keywords:
Surface ozone variation
GAW stations
Regional representativeness
Asian summer monsoon

ABSTRACT

Six World Meteorological Organization (WMO)/Global Atmosphere Watch (GAW) stations are located at background sites in China, which constitute a network for monitoring surface ozone, including its long-term temporal variation. In this study, we evaluated the seasonal variation in surface ozone simulated by the ECHAM/MESSy Atmospheric Chemistry (EMAC) general circulation model with the measurements made at these WMO/GAW background stations for the period of 2010–2012, and investigated the regional representativeness of each station with respect to the seasonal variation in surface ozone. We determined the contributions of ozone originating from various tropospheric and stratospheric latitude bands based on EMAC simulations using a tagged tracer approach. The results showed that the predominant contribution to surface ozone was from the troposphere in northern middle-high and tropical latitudes. For each station there was a large surrounding area in which the yearly ozone maximum occurred in the same month as it did at the station, reflecting the regional characteristics of the seasonal variation in surface ozone recorded at the WMO/GAW background stations. Surface ozone in China was found to generally peak in summer over non-monsoon and mid-latitude monsoon regions and in spring over low-latitude monsoon regions, indicating that the regional representativeness of ozone variability in China is significantly influenced by the Asian summer monsoon.

1. Introduction

Ozone is a central trace gas in tropospheric photochemistry. As the major precursor of hydroxyl radical (OH), ozone concentrations affect the lifetime of a large number of trace gases through photolysis (Levy, 1971; Weinstock and Niki, 1972; Wofsy et al., 1972). Ozone acts as a greenhouse gas with the third strongest warming effect after carbon dioxide (CO_2) and methane (CH_4) (IPCC, 2007). In addition, ozone is an efficient oxidant and plant toxicant, and has a negative impact on human health and terrestrial vegetation (Heck et al., 1982; Lee et al., 1996; Shindell et al., 2012).

Key factors that influence the levels of ozone in a specific region include its photochemical production and destruction, stratosphere-to-troposphere transport, and inflows and outflows of air pollution via long-range transport (Lelieveld and Dentener, 2000). While pollution episodes usually happen in populated and industrialized areas, high concentrations of ozone and its precursors can occur due to transport through atmospheric circulations, influencing the tropospheric ozone levels downwind of the emission sources. Research over the past two decades has clearly shown that ozone and its precursors are regularly

* Corresponding author.
E-mail address: majz@cma.gov.cn (J. Ma).

https://doi.org/10.1016/j.atmosenv.2020.117672
Received 27 March 2020; Received in revised form 1 June 2020; Accepted 3 June 2020
Available online 9 June 2020

exported from their emission source to receptor regions far downwind on the regional, intercontinental, and even hemispheric scale (HTAP, 2010; Monks et al., 2009; Stohl, 2004). These transport pathways are predominantly from west to east at mid-latitudes, with *in situ* and satellite-based observations showing that pollution plumes (anthropogenic and biomass burning) not only travel from North America to Europe, or from East Asia to North America, but can also circle the globe (Jacob et al., 1999; Jaffe et al., 1999; Lewis et al., 2007; Wild et al., 2004).

China has a pronounced monsoon climate, with the Asian monsoon affecting the meteorology by changing atmospheric circulations, water vapor, clouds and radiation, influencing the seasonal and spatial contributions of ozone and its precursors by dilution, transport, photochemistry, and deposition processes. Ozone levels in China are affected mostly by the Asian summer monsoon (ASM) that prevails during June and August, providing various transport pathways of ozone and its precursors. First, moist air masses containing low levels of ozone are transported from the northwest Pacific Ocean to southern China through ASM circulations, and there is also an ozone suppression effect due to increased cloudiness and precipitation, resulting in low ozone levels in southeast China (He et al., 2008; Liu et al., 2009; Ma et al., 2002a; Safieddine et al., 2016; Tang et al., 2013; Zhao et al., 2010). For example, Zhou et al. (2013) conducted a study in Hong Kong and Tang et al. (2013) undertook research at an agricultural site in Yangtze River Delta, and both studies have reported an ozone decline in summer that was associated with an influence from marine air masses. In addition, the South Asian summer monsoon (SASM), which is linked to the ASM (the other part being the East Asian monsoon), transports pollution plumes that enhance the ozone levels of the southeastern Tibetan Plateau in spring (Ma et al., 2014; Yin et al., 2017). Ma et al. (2014) conducted *in situ* observations and plume trajectory model simulations, which showed that polluted plumes from southern Asia before or at the beginning of the ASM season led to a spring ozone maximum in Xianggelila, a station located in the southern Tibetan Plateau, while the increased cloud cover and precipitation along with the decrease in the mixing layer height as a result of the ASM led to an ozone minimum during summer. In addition, because of the ASM circulation, pollution plumes are transported to downwind regions from the industrial cities in southeastern and central China, reaching areas of northern and northeastern China that are less affected by the ASM and leading to a gradual northward enhancement of background ozone levels in eastern China (He et al., 2008; Liu et al., 2019; Liu and Ma, 2017; Ma et al., 2002a).

Network monitoring has provided a basis to study the spatial distribution and long-term temporal variation in surface ozone. The WMO/GAW has been one of the key international initiatives in the long-term monitoring chemical and physical properties of the atmosphere. In China, there are six WMO/GAW stations, including one global (Waliguan) and five regional (Xianggelila, Akedala, Lin'an, Shangdianzi, and Longfengshan) stations, which are hereafter referred to as WLG, XGLL, AKDL, LN, SDZ, and LFS, respectively. WLG, XGLL, and AKDL are in remote areas of western China, with WLG and XGLL located in the northeast and southeast of the Tibetan Plateau, respectively, and AKDL located in northwestern China. LN, SDZ, and LFS are located in eastern China. Long-term observations at the six stations have shown that the levels of ozone differ not only among stations but also seasonally at the same station (Lin et al., 2008, 2010; Liu et al., 2019; Ma et al., 2002b, 2014, 2016; Xu et al., 1998, 2008, 2009, 2016; Xue et al., 2011; Zhu et al., 2004). Compared to other stations, surface ozone levels at WLG are higher throughout the year, with a peak in summer, the reasons for which are under debate (Ding and Wang, 2006; Li et al., 2009; Ma et al., 2002a, 2002c, 2005; Xue et al., 2011, 2013; Yang et al., 2014; Zhu et al., 2004).

XGLL exhibits an ozone mixing ratio trough in summer, as a result of fewer ozone containing air masses and much more cloud cover and precipitation caused by the ASM (Ma et al., 2014). Persistent enhanced ozone levels have been observed at AKDL from February to June, due to strong stratospheric ozone intrusions in spring at high latitudes (Hsu and Prather, 2009), followed by a decline in July. There are two peaks at Lin'an during the year: A major peak in May and a minor peak in October, which are associated with active photochemical production in the spring and autumn over the surrounding region (Xu et al., 2008). Compared to other stations, the summer ozone mixing ratios at Lin'an are lower, mainly due to the influence of clean marine air masses from the northwestern Pacific brought by the ASM (Ma et al., 2002c). Surface ozone at SDZ shows a summer peak in the annual cycle. Under the control of the ASM, ozone and its precursors are transported continuously from the southwest of North China to the station and they accumulate in the SDZ region. This accumulation is accompanied by photochemical production (Lin et al., 2008; Liu and Ma, 2017; Sun et al., 2016; Wang et al., 2006; Xu et al., 2011). Similarly, LFS has an ozone peak in June due to the influence of transport from North China and the mid-southern region of northeast China (Liu and Ma, 2017; Xu et al., 2009). Although ozone variation at these GAW stations has taken on regional characteristics, it is still not clear that to what extent the area surrounding a specific station can show the same seasonal ozone variation as the station itself and what are the dominant sources of the ozone contributing to the regional surface ozone in the various seasons.

Generally, the factors controlling the seasonal variation in surface ozone is different between western and eastern China. Surface ozone levels in western China are primarily influenced by atmospheric dynamics and long-range transport, whereas in eastern China they are controlled by photochemistry and regional pollution transport (Ma et al., 2002c). Compared to western China, eastern China has lower background ozone levels. However, the ASM can transport photochemical pollutants from the southern to northern areas of eastern China, leading to a northward gradual enhancement of background ozone levels at the eastern GAW stations (Liu et al., 2019). Modeling studies of surface ozone in China have mainly focused on local photochemical or regional chemical reactions and transport, paying less attention to the contributions of background ozone transported from long distances outside China. Some studies report that ozone exported from Europe and North America reaches a minimum in summer, while the ozone exported from southeast Asia exhibits a maximum in summer over eastern China, and the seasonal switch in monsoonal wind patterns plays a significant role in determining the seasonal background ozone in China (Wang et al., 2011). Others concluded that Europe (particularly during spring and summer) has the largest impact on China's surface ozone, followed by India, the Middle East, Southeast Asia, Siberia, and mid-Asia (Li et al., 2014). It was also found that North American ozone mainly influences northern China (>30°N) with the peak in winter and trough in summer, and limited influence on southern China (<30°N) (Zhu et al., 2017). In view of these ambiguities, the influence of ozone from various sources on the seasonality in various regions of China needs further analysis.

In this study, we investigated the contributions of ozone originating from various latitude bands to the seasonal variation in surface ozone at the six GAW stations in China, and explored the regional representativeness of each station using the ECHAM/MESSy Atmospheric Chemistry (EMAC) general circulation model. Section 2 describes the EMAC model used in this study and the six GAW stations in China, and Section 3 evaluates the ability of EMAC to simulate the seasonal variation in background surface ozone in China. In section 4, we show the seasonal variation in the influence of ozone originating from various latitude bands, as tagged in EMAC, on surface ozone at the six GAW stations. In Section 5, we present the regional representativeness of each station for surface ozone seasonal variation. The conclusions are given in Section 6.

2. Observational data and model

2.1. GAW stations in China

The geographical locations, latitudes, longitudes, and altitudes of the

six Chinese GAW stations are shown in Fig. 1. WLG was established in 1989 and is located in Qinghai Province. It is one of global baseline stations in the WMO/GAW network and the only one in the hinterland of the Eurasian continent. WLG is situated on the summit of Mount Waliguan at the northeastern edge of the Tibetan Plateau in an area with a very low population density, little industry, and other anthropogenic sources of ozone precursors within 30 km. However, some impact of the long-range transport of anthropogenic pollutants from the NE–SE sector cannot be excluded, particularly from the major cities of Xining (about 90 km northeast of WLG, with a population of around 2.13 million) and Lanzhou (about 260 km east of WLG, with a population of around 3.1 million). Such impacts, if they occur, may be significant only during the warm period (May–September) (Ma et al., 2002b; Xu et al., 2016).

XGLL was established in 2006 and is located about 450 km northwest of Kunming in Yunnan Province at the southeastern rim of the Tibetan Plateau. It is considered weakly affected by local anthropogenic activities because there is almost no significant anthropogenic source of ozone precursors surrounding the station and the nearest township, Xianggelila, is about 30 km from the station. The climatology at XGLL is mainly controlled by the ASM circulation that brings abundant precipitation (Ma et al., 2014).

AKDL was established in 2006 and is located in the Xinjiang Autonomous Region about 30 km from the nearest township in the northwest direction. The prevailing wind is from the SE sector in winter and NW sector in other seasons (Lin et al., 2010).

LN was established in 1983 and is located in the Yangtze River Delta, one of the leading regions of China in terms of economic growth. There are a few large cities in the sector to the E–NNW of LN, with the nearest and largest being Hangzhou (about 50 km to the east) and Shanghai (about 210 km to the northeast), respectively. About 10 km to the south of LN is the Lin'an Township, with a population of approximately 50,000. It has a typical subtropical monsoon climate, with distinctive seasonal characteristics (Wang et al., 2001; Xu et al., 2008).

SDZ was established in 1981 and is located in the northern part of the North China Plain in the Miyun County of Beijing. It is about 100 and 55 km northeast of the urban areas of Miyun Township and Beijing, respectively. Within 30 km of the site, there are only small villages in mountainous areas with a sparse population and insignificant anthropogenic emission sources. SDZ has a semi-moist monsoon climate and the prevailing winds are from the NE and SW sectors (Lin et al., 2008).

LFS was established in 1981 and is located on the edge of the Changbai Mountains and at the southeastern edge of the Songnen Plain. LFS is 2 km from the nearest township and there are no significant industrial emissions in the surrounding area (Xu et al., 1998). The main pollution transport occurs from the S–SW sectors at low latitudes, although wind speeds are low (Xu et al., 2009).

2.2. Model description and configuration

The EMAC model is a chemistry–climate model that combines the 5th generation European Centre-Hamburg general circulation model (ECHAM5) with the Modular Earth Submodel System (MESSy) Atmospheric Chemistry system (Jöckel et al., 2006, 2010) to simulate and predict atmospheric processes from the troposphere to middle atmosphere and their interactions with land and oceans. EMAC has been extensively used at a range of spatial resolutions and has been evaluated against surface site, aircraft, and satellite measurements of trace gases and aerosols in both the troposphere and stratosphere (Brühl et al., 2012; Jöckel et al., 2006; Kirner et al., 2010; Lelieveld et al., 2007; Pozzer et al., 2012). ECHAM is based on the temperature, vorticity, divergence, and surface pressure in spectral coordinates, and specific humidity, cloud water, and cloud ice in grid point coordinates, with a mix of coordinates in the vertical direction (Jöckel et al., 2005). MESSy submodels calculate atmospheric chemical concentrations (Sander et al., 2005), aerosol loadings (Kerkweg et al., 2007; Pringle et al., 2010; Tost and Pringle, 2012), cumulus convection (Tost et al., 2006), pollutant emissions, vegetation emissions, and ozone tagging via ozone tracers produced in different regions at various latitudes and altitudes (Jöckel et al., 2016). For this study, we used version 5.3.02 of ECHAM5 and version 2.52 of MESSy, the emission inventory of which is the Representative Concentration Pathways scenario 8.5 (RCP8.5) for fossil fuel combustion and biomass burning emissions (Jöckel et al., 2016). The

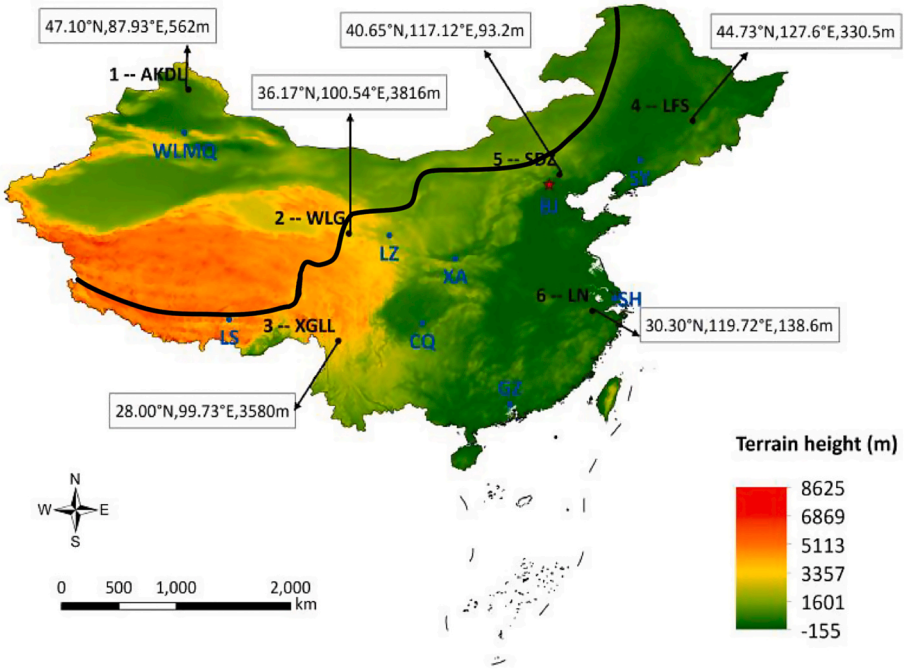

Fig. 1. Six GAW stations in China. The black line distinguishes the area affected by the monsoon (the east part) from the non-monsoon region (the west part). Blue dots refer to major cities including Shenyang (SY), Beijing (BJ), Shanghai (SH), Wulumuqi (WLMQ), Lanzhou (LZ), Xi'an (XA), Lasa (LS), Chongqing (CQ), and Guangzhou (GZ). (For interpretation of the references to colour in this figure legend, the reader is referred to the Web version of this article.)

RCP8.5 global emission inventory has a horizontal grid resolution of 0.5° × 0.5° at monthly intervals and vertical distributions as described in Pozzer et al. (2009). The monthly cycle of RCP8.5 emissions in 2010 was used in this study. The natural emissions of non-methane hydrocarbons (NMHCs) were based on the Global Emissions InitiAtive (GEIA) database (Bouwman et al., 1997). Nitrogen oxides (NO_x) produced by lightning were calculated online and distributed vertically based on the parameterization of Pringle et al. (2010). The nitric oxide (NO) emissions from soils were calculated online according to the algorithm used by Yienger and Levy II (1995).

In this study we performed a 3-year simulation for the period from 2010 to 2012 with EMAC, with a strong ASM year in 2010 and weaker ASM years in 2011 and 2012 (China Meteorological Bureau, 2015). Thus, the results reflect the influence of typical atmospheric circulation patterns on global pollutant transport. In accord with the modeling scheme of Ma et al. (2019), the model spectral resolution used in this study was T106L90, which corresponds to a horizontal grid resolution of approximately 1.125° × 1.125° and 90 vertical layers extending from the surface to an altitude of 0.01 hPa (~80 km). In the simulation, the meteorology was nudged by Newtonian relaxation towards the European Centre for Medium-Range Weather Forecasts (ECMWF) operational re-analysis data for the period of 2010–2012. The prognostic variables nudged towards the realistic meteorological conditions (i.e., the re-analyses) were temperature, vorticity, divergence, and surface pressure, and the nudging weights were chosen such that the mesosphere and upper stratosphere and the boundary layer were not directly influenced (Lelieveld et al., 2007). The nudging was exerted with maximum weights at the model levels from 37 (~10 hPa) to 83 (~706 hPa), leaving the highest thirty (upper middle atmosphere) and the lowest three (boundary layer) model levels free (apart from surface pressure).

3. Model evaluation

Jöckel et al. (2016) showed that all free-running simulations by EMAC overestimated tropospheric partial column ozone during 1980–2011 (by up to 3% in the tropics), and the mean biases were largely reduced by including the model nudging to global temperature fields. Evaluations of surface ozone levels in China based on EMAC have not been conducted so far. Among the six Chinese GAW stations, similar evaluations in China based on other atmospheric chemistry models have only been conducted at WLG (Li et al., 2009; Ma et al., 2002b, 2002c, 2005; Zhu et al., 2004) and LN (Wang et al., 2011).

Due to the elevation differences between the GAW stations and model terrain, it is necessary to take the altitudes of the various vertical layers in EMAC into account, even though the model applies a terrain-following coordinate system near the surface (shown in Table 1). The altitudes of the four low surface stations (AKDL, LFS, SDZ, and LN) in the model grid at the lowest (90th) layer were very close to their respective real altitudes, while the altitudes of the elevated stations were closer to the height of the 89th layer (the second lowest layer) for WLG and the height of the 88th layer for XGLL. However, simulated ozone concentrations at the 90th layer appeared to be more representative to surface observations than those simulated at the 89th and 88th layers for WLG and XGLL, respectively (not shown). Furthermore, the regional distributions of the simulated ozone concentrations differed little among the 90th, 89th, and 88th layers (figures for the 89th and 90th layers are not shown). Therefore, in this study we used the calculated results at the 90th layer in EMAC, i.e. the middle of the lowest layer of about 60 m, to conduct the following analyses. Monthly surface ozone mixing ratios for the years 2010–2012 at WLG, XGLL, AKDL, LFS, SDZ, and LN between the simulation and *in situ* observations are shown in Fig. 2. The simulated results were shown to successfully reproduce surface ozone levels and their seasonal variation at the stations. The simulated monthly ozone levels at SDZ and LN were very close to the observations, and the simulated monthly ozone levels at WLG, XGLL, and LFS had similar seasonal variation patterns to the observations. Ozone levels in spring and summer were overestimated at all stations except LN, which might result from a common bias in atmospheric chemistry models due to their limitations in reproducing cumulus convection (Ma et al., 2002a) and ASM (Li et al., 2014; Wang et al., 2009), or a bias associated with the boundary layer parameterization (Jöckel et al., 2016; Liu et al., 2006).

The correlation coefficients for the relationship between simulated and observed monthly surface ozone concentrations were 0.94, 0.91, 0.90, 0.88, 0.78, and 0.49 at SDZ, LN, WLG, XGLL, LFS, and AKDL, respectively. These significant associations confirmed that the simulated surface ozone concentrations could reflect the seasonal variation in surface ozone at the Chinese GAW stations.

4. Source tagging on surface ozone at the Chinese GAW stations

The characteristics of the six Chinese GAW stations, i.e., geographic location, altitude, and the predominant source of polluted air masses and hence the relative influence of anthropogenic sources are mentioned in section 2.1. Because the levels of ozone in various source regions are different and ozone may undergo diverse chemical and physical processes during long-range transport, trajectory analyses is limited in determining the ozone sources at a station. One the other hand, the method of simply adding/omitting a certain pollutant source has been widely used in model studies of tropospheric ozone, particularly its perturbation by human activities. However, the turning on and off method is not so efficient in the study of various processes in a specific atmosphere. For instance, if one investigates the significance of stratospheric ozone intrusions to the source of tropospheric ozone using turning on and off method, it would be difficult to quantify the relevant contribution, since the concept of the atmosphere with stratospheric ozone source being turned off is not clear. An atmospheric chemistry–general circulation model (AC-GCM) can be a useful tool for the quantitative calculation of ozone fields originating from various sources. In an AC-GCM, tagging a pollutant from specific sources can identify the relative contributions of various sources to tropospheric pollutant levels. Tagging simulations are superior to the method of simply opening/closing a certain pollutant source due to the constant physical and chemical features after tracers are included in the model, which may provide more robust results (Ma et al., 2002c).

Ozone tagging simulations by EMAC were conducted via 14 ozone tracers (O3ONHTS, O3OTRTS, O3OSHTS, O3ONPLS, O3ONMLS, O3OTRLS, O3OTRMS, O3OSMLS, O3OSPLS, O3ONPUS, O3ONMUS,

Table 1
Locations and altitudes of the six Chinese WMO/GAW stations.

Station name	Abbreviation of station name	Latitude (°E)	Longitude (°N)	Altitude (m)	Model terrain altitude (m)	Model layer altitude (m) above ground		
						90th layer	89th layer	88th layer
Akedala	AKDL	87.93	47.10	562.0	518.53	29.74	/	/
Waliguan	WLG	100.54	36.17	3816.0	3624.66	30.30	135.89	/
Xianggelila	XGLL	99.73	28.00	3580.0	3099.86	31.07	140.92	377.09
Longfengshan	LFS	127.60	44.73	330.5	302.10	29.03	/	/
Shangdianzi	SDZ	117.12	40.65	93.2	158.13	29.56	/	/
Lin'an	LN	119.72	30.30	138.6	141.39	31.62	/	/

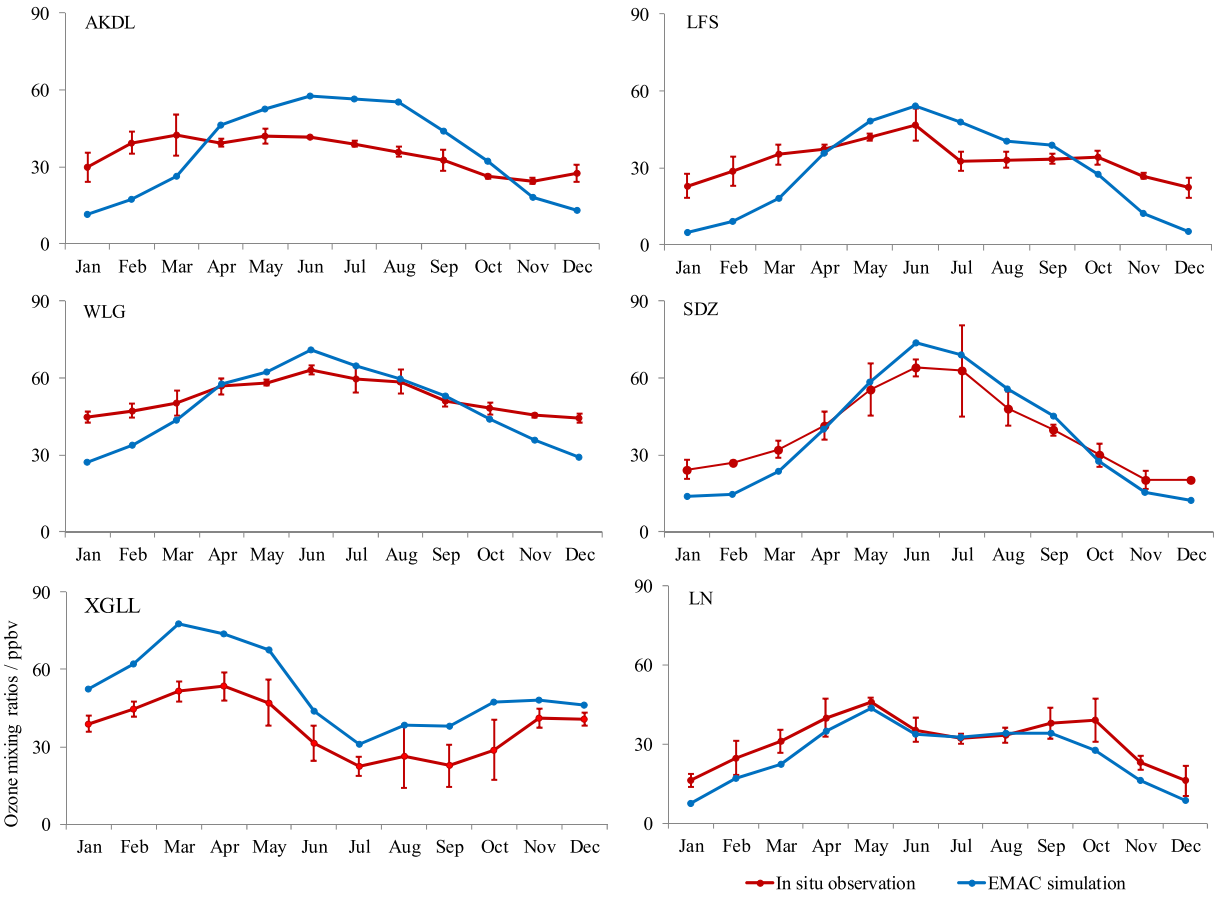

Fig. 2. Comparisons of the monthly surface ozone mixing ratios (unit: ppbv) between the EMAC simulation (blue line) and *in situ* observations (red line, vertical bars are standard deviations) at each GAW station during 2010–2012. (For interpretation of the references to colour in this figure legend, the reader is referred to the Web version of this article.)

O3OTRUS, O3OSMUS, and O3OSPUS) that formed at various latitudes and altitudes. Each ozone tracer was produced only in one specific region: northern mid-high latitudes troposphere (NHTS), tropical troposphere (TRTS), southern mid-high latitudes troposphere (SHTS), northern polar lower stratosphere (NPLS), northern mid-latitudes lower stratosphere (NMLS), tropical lower stratosphere (TRLS), tropical middle stratosphere (TRMS), southern mid-latitudes lower stratosphere (SMLS), southern polar lower stratosphere (SPLS), northern polar upper stratosphere (NPUS), northern mid-latitudes upper stratosphere (NMUS), tropical upper stratosphere (TRUS), southern mid-latitudes upper stratosphere (SMUS), and southern polar upper stratosphere (SPUS) (Grewe, 2006; Jöckel et al., 2016).

To determine the contributions of ozone from various source fields at each Chinese GAW station, we further combined the stratospheric fields at each latitude, defining the NMLS and NMUS as the northern mid-latitudes stratosphere (NMST), the NPLS and NPUS as the northern polar stratosphere (NPST), and the TRLS, TRMS, and TRUS as the tropical stratosphere (TRST), respectively. All southern hemispheric fields were ignored due to their negligible contributions to the ozone levels in China. Then the ozone source fields were divided into five sections, i.e., the NHTS, TRTS, NMST, NPST, and TRST, as shown in Table 2. Note that the top boundary of TRTS is higher (100 hPa) than that of NHTS (200 hPa), and the two tropical regions of TRTS and TRST have different latitude and longitude ranges. The percentage contributions of the five ozone tracers to surface ozone at the six Chinese GAW stations are presented in Fig. 3 for hourly values and Table 3 for 3-year mean plus/minus standard deviation values. In general, the NHTS and TRTS were the predominant contributors to surface ozone at each station. As in previous studies (Lin et al., 2010; Ma et al., 2002a, 2002c, 2014; Xu et al., 1998), our results showed that the contributions from stratosphere-troposphere exchange (STE) to surface ozone were not ignorable, with the NMST presenting the most significant contribution at AKDL and WLG (more than 7%), and the NPST presenting the most significant contribution at LFS (approximately 3%). LFS received more ozone from the stratospheric fields than the other stations because it is located in an area directly below the jet stream, and is therefore significantly influenced by the ozone transported downward in synoptic weather systems (Ma et al., 2002c).

Table 2
Five ozone sources tagged in the EMAC.

Abbreviation of ozone source	Full names of ozone source	Latitude	Altitude
NHTS	Northern mid-high latitudes troposphere	30.7–90.0°N	≥200 hPa
TRTS	Tropical troposphere	30.7°S-30.7°N	≥100 hPa
NMST	Northern mid-latitudes stratosphere	19.5–61.4°N	<200 hPa
NPST	Northern polar stratosphere	61.4–90.0°N	<200 hPa
TRST	Tropical stratosphere	19.5°S-19.5°N	<100 hPa

Because the stratospheric sources contributed less than the tropospheric sources, we further combined the NMST, NPST, and TRST to represent the whole stratosphere (ST). Fig. 4 presents the contributions of the NHTS, TRTS, and ST tracers to the monthly variability in surface ozone at the six Chinese GAW stations. Surface ozone levels at AKDL

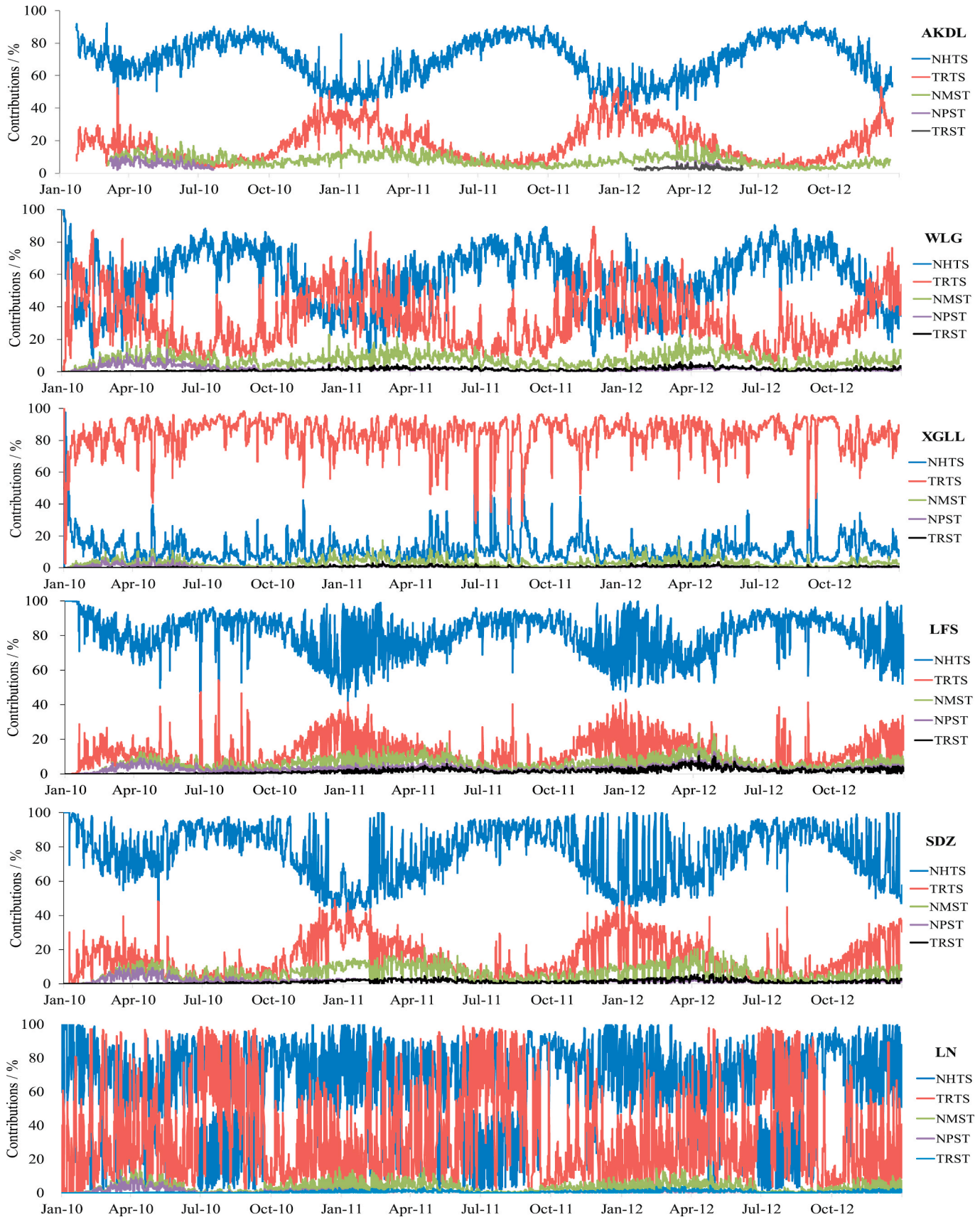

Fig. 3. Hourly contributions (unit: %) from various ozone sources to the surface concentration at each Chinese GAW station during 2010–2012.

Table 3
Percentage contributions (3-year mean and standard deviation) of the five ozone tracers (see Table 2) to the surface ozone concentrations at the six Chinese GAW stations.

	NHTS	TRTS	NMST	NPST	TRST
AKDL	70.23 ± 13.53	17.60 ± 11.19	7.33 ± 3.34	2.74 ± 1.66	1.62 ± 1.03
WLG	58.17 ± 17.37	31.44 ± 16.67	7.07 ± 3.57	1.79 ± 1.49	1.36 ± 1.00
XGLL	11.61 ± 8.51	83.88 ± 10.14	3.06 ± 2.17	0.68 ± 0.70	0.58 ± 0.55
LFS	79.56 ± 11.09	12.11 ± 8.18	5.23 ± 2.92	1.26 ± 1.23	1.70 ± 1.40
SDZ	76.77 ± 14.96	14.18 ± 10.73	6.11 ± 4.05	1.63 ± 1.41	1.22 ± 1.03
LN	61.56 ± 24.83	33.64 ± 25.77	3.24 ± 2.75	0.87 ± 1.08	0.63 ± 0.64

predominantly originated from the NHTS, with significant seasonal variability, i.e., higher contributions in summer and lower ones in winter. They were also weakly influenced by the TRTS and ST, with a peak contribution in spring. Similarly, surface ozone at WLG predominantly originated from the NHTS, with a summer peak, and some contribution from ST from late spring to early summer. Surface ozone at XGLL predominantly originated from the TRTS, with a maximum in spring and a minimum in summer. This was because XGLL is located at a low latitude and is generally influenced by low level ozone air masses that accompany the ASM (Ma et al., 2014). Surface ozone at the three stations in eastern China also predominantly originated from the NHTS. The summer peaks at LFS and SDZ were due to the significant photochemical formation and transport of ozone in the troposphere at northern mid-high latitudes (Lin et al., 2008; Liu and Ma, 2017; Xu et al., 2009, 2011). For LN, the primary and secondary peaks of the NHTS contributions occurred in spring and autumn, respectively, resulting from the local intensive photochemical formation of ozone (Xu et al., 2008). In general, surface ozone at the six Chinese GAW stations is influenced by ST with peak contributions during April and June, later than the peak contributions during February and March at a mid-latitude station, Goose Bay, shown by Wang et al. (1998), who performed a 1-year simulation for the 1990s with a global three-dimensional chemistry-transport model including separate tracers for ozone produced in the stratosphere and in different regions of the troposphere.

5. Regional representativeness of surface ozone at the Chinese stations

5.1. Seasonal variation in surface ozone

Large parts of China are under the influence of the Asian monsoon. The northernmost border of the ASM region, which is bounded by the Daxingan, Yinshan, Helan, Bayankala, and Gangdise mountains, is generally considered the boundary between the monsoon and non-monsoon regions (see Fig. 1). The area east and south of the line is the monsoon region (MR), while the remaining area is the non-monsoon region (NMR) (He et al., 2012). Based on the position of this boundary, we further defined that in China, 0–30°N represented the low-latitude MR (LMR), 30–55°N represented the mid-latitude MR (MMR), and the remaining area was the NMR.

Calculated monthly variation in surface ozone mixing ratios and wind fields at 850 hPa (the altitude where the ASM appears most significantly) during 2010–2012 over China are shown in Fig. 5. Generally, surface ozone concentrations were lower in winter and higher

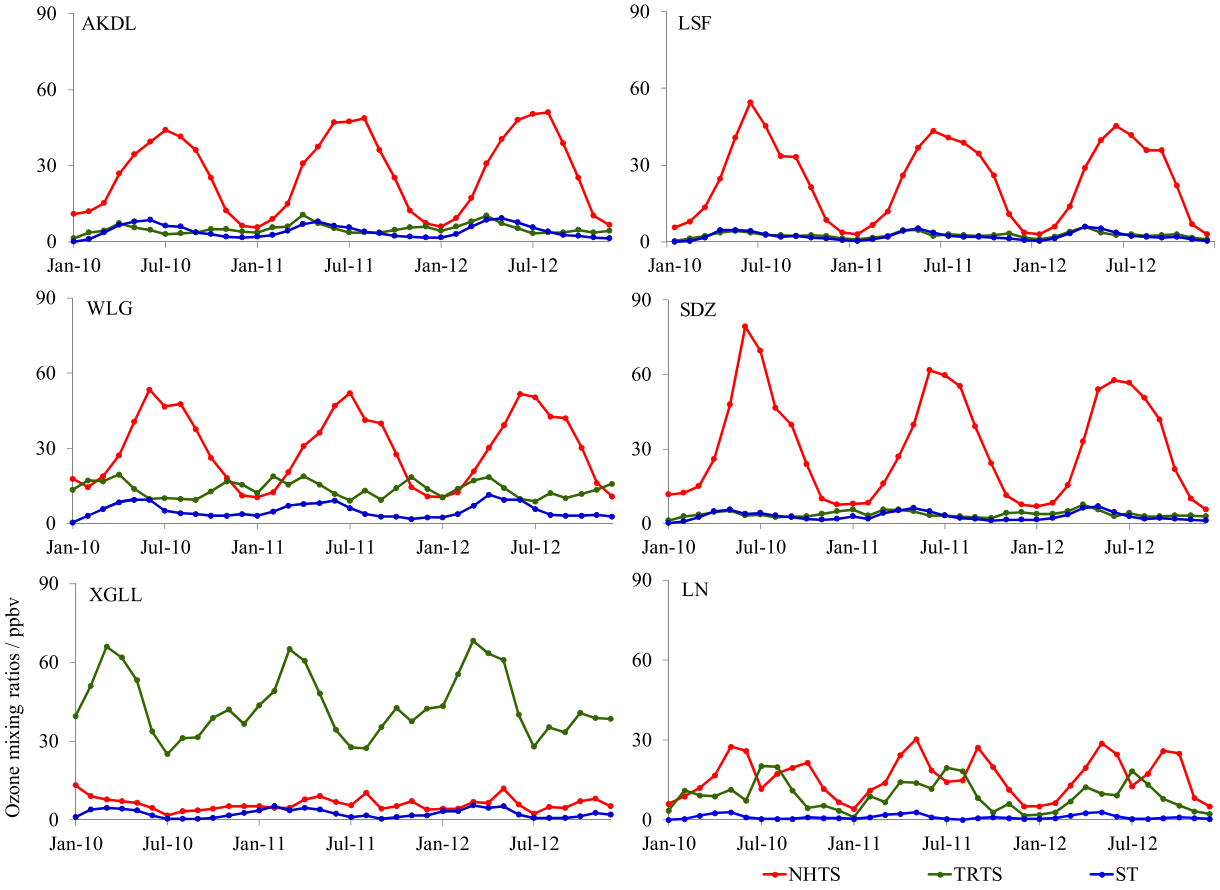

Fig. 4. Contributions of various ozone tracers to monthly variability in surface mixing ratios (unit: ppbv) at each Chinese GAW station during 2010–2012.

in spring and summer. Geographically, ozone levels were higher in western China and lower in eastern China (except for summer), with a year-round high level over the Tibetan Plateau. Compared to western China, eastern China experienced more significant seasonal variation in surface ozone. Ozone over the MMR reached a maximum in June, with a high concentration centre in the North China Plain, which proceeded northward in July under the influence of the ASM.

Fig. 6 shows the regional distribution of the month during which the maximum surface ozone concentration occurred, determined from the calculated monthly results for 2010. The influence of the ASM on surface ozone variation in China can be clearly seen in the figure, with the maximum appearing in spring within the LMR and in summer within the MMR and NMR. Over the Tibetan Plateau, an ozone maximum was apparent from south to north from March to June. WLG and the surrounding area in the northeast-southeast direction, which is located at the northeastern edge of the Tibetan Plateau within the MMR, experienced an ozone maximum in June. XGLL and a large region to its south, which is located in the southern Tibetan Plateau within the LMR, had an ozone maximum in March during the onset of the SASM. AKDL, together with a large region to its south, which is located within the NMR, experienced an ozone maximum in July. In eastern China, ozone levels at LN and the area within a distance of 200 km experienced an ozone peak in May, near the onset of the East Asia summer monsoon (EASM). Ozone at SDZ and the whole of the North China Plain and at LFS together

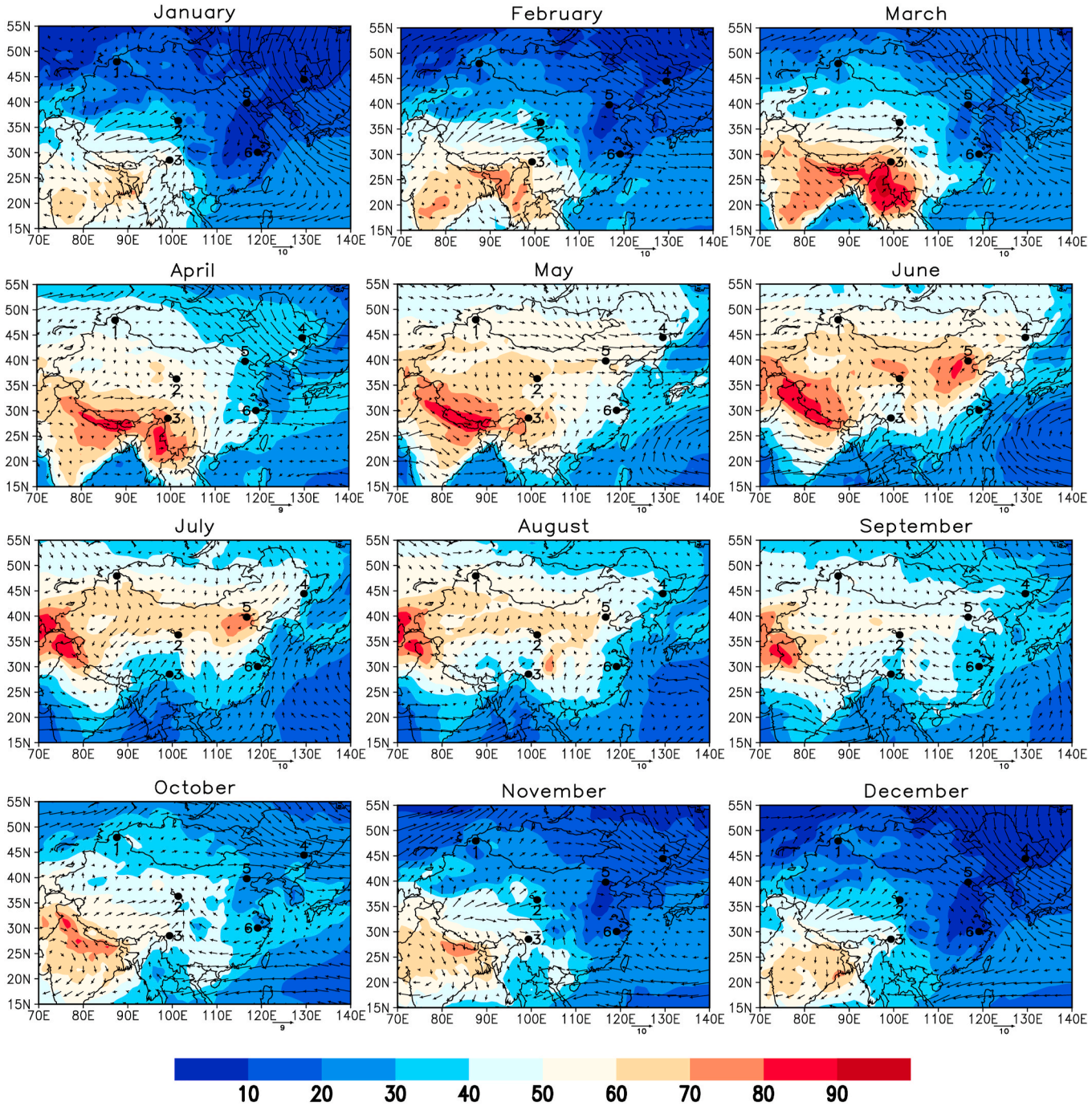

Fig. 5. Simulated regional distributions of monthly surface ozone mixing ratios (shaded, unit: ppbv) in China and the overlayed wind fields (vectors) at 850 hPa during 2010–2012. Numbers represent the six GAW stations shown in Fig. 1.

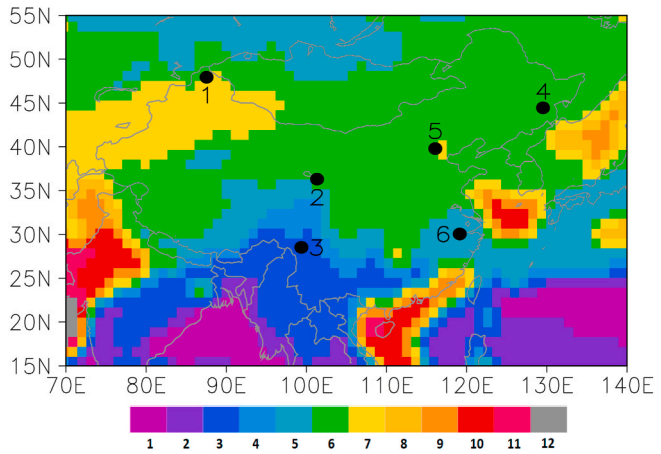

Fig. 6. Regional distribution of the month of occurrence of the maximum surface ozone concentration in each grid in an annual cycle in 2010. Numbers represent the six GAW stations shown in Fig. 1.

with the whole of the Northeast China Plain, both of which are located in the MMR, consistently peaked in June.

5.2. Contributions of various ozone sources

The regional distributions of tagged ozone from the three sources (NHTS, TRTS, and ST), as described in Section 4, at the surface for each month are presented in Figs. 7–9, respectively. In the MMR, ozone was predominantly from the NHTS, which peaked in June, with a maximum of 30–75 ppbv. In the same month, ozone from the NHTS contributed over 50 ppbv to the levels at SDZ and the whole of the North China Plain, and accounted for 90–95% of the surface ozone concentration. It contributed homogeneously to levels at LFS and the middle-south area of the Northeast China Plain, with concentrations between 50 and 60 ppbv, accounting for around 91% of surface ozone concentration. This matched the percentage contribution from ozone photochemical production in the summer of 1995 over China, which was simulated previously using a tagging method (Ma et al., 2002c). It was found that the NHTS made a predominant contribution to the ozone levels in the MMR of China, with the main sources being from the region itself. In addition, polluted air masses in the MMR can be transported downwind by ASM circulations and increase the background ozone levels in downstream regions (Ma et al., 2002c).

In June, ozone from the NHTS contributed 50–60 ppbv (70–75%) to the levels at WLG and its surrounding area in the northeast-southeast direction. The ozone from the TRTS and ST contributed 10–15 ppbv (14–18%) and 8–10 ppbv (less than 12%), respectively. The contribution from the ST at WLG estimated in this study was less than half of that reported by Ma et al. (2002c), who estimated a 28% contribution. Ozone from the stratosphere contributed much more to ambient levels over the Tibetan Plateau than in other regions, particularly during spring and summer, with contributions up to 14 ppbv over the western part of the Tibetan Plateau with a percentage of approximately 20%. Compared with the results of Wang et al. (1998), ozone from the stratosphere in this study contributes much less to mid-latitudes, especially in winter.

Unlike the MMR, ozone in the LMR was not dominated by NHTS sources. In May, the ozone contribution from the NHTS (20–25 ppbv, accounting for about 51%) to the levels at LN and the region approximately 300 km to its south and west was slightly higher than that from the TRTS (15–20 ppbv, accounting for about 38%), the sum of which was far more than the contribution from the stratosphere. The ozone contributions at LN are in accord with those found by Ma et al. (2002c). In March, ozone from the TRTS made the dominant contribution at XGLL and a large region to the south of the station, with a maximum of more than 60 ppbv (>84%), whereas the NHTS contributed less than 10 ppbv (<12%). The ST contributed less to this region than to the rest of the Tibetan Plateau region (including WLG). Surface ozone concentrations in the LMR, particularly over the southern Tibetan Plateau, were significantly influenced by ozone from the tropical troposphere over south and southeast Asia. The results agree with those of Li et al. (2014), i.e., indicating that emissions from India increase surface ozone most significantly towards the southern part of the Tibetan Plateau during spring.

In July, ozone from the NHTS contributed to the levels at AKDL, and at the local scale it contributed to the ozone peaks south of the station during the year by more than 45–50 ppbv (>70%), being far more than the contributions from other sources. Figs. 7–9 also show that compared to the relatively small region surrounding AKDL, larger areas in the south received contributions from all three ozone sources, including the NHTS, explaining the particular ozone variation at AKDL and the small region surrounding the station. In general, ozone from troposphere contributes much more than shown by the results of Wang et al. (1998) with percentages of 10–50%.

Fig. 10 shows the regional distributions of the month in which the maximum monthly average surface concentration of tagged ozone on each grid in 2010 occurred for the three ozone sources, i.e., NHTS, TRTS, and ST, respectively. The regional representativeness of the contributions for various ozone sources at the GAW stations was identified. The overall distribution pattern of the month of occurrence for the maximum tagged ozone concentration from the NHTS (Fig. 10a) strongly resembled that for the regular ozone concentration shown in Fig. 6. There was a single significant discrepancy in that ozone from the NHTS was most significant in August over the region south of AKDL (Fig. 10a), whereas the total ozone concentration was most significant in July over the large region around AKDL (Fig. 6). It was concluded that the "August maximum region" was the result of ozone transport from the Middle East or to a lesser degree Europe, in agreement with the results of Li et al. (2014), i.e., influence from mid-Asia and Europe to western China peaked in spring and summer. The maximum monthly ozone concentration from the NHTS consistently occurred in June over large regions, including SDZ and the whole of the North China Plain, LFS and the large region in the middle-south of the Northeast China Plain, and WLG and the surrounding area in the northeast-southeast direction. This indicates that the stations in the MMR are regionally representative with respect of the seasonal variation in ozone from the NHTS. Similarly, the maximum monthly ozone from the NHTS occurred in May at LN and the surrounding area and in July at the AKDL, together with the region to the east and southeast of the station, reflecting the regional representativeness of LN and AKDL for the seasonality in ozone levels originating from the NHTS. The maximum monthly ozone contributions from the TRTS (Fig. 10b) and ST (Fig. 10c) at XGLL and the large region to the south of the station occurred in March, reflecting the regional representativeness of XGLL for the seasonality in ozone levels from the TRTS and the whole ST in the southern part of the Tibetan Plateau.

6. Conclusions

We investigated the regional representativeness of the Chinese GAW stations with respect to the seasonal variability in surface ozone using the EMAC model. The ozone contributions originating from various tropospheric and stratospheric latitude bands, simulated by EMAC using the tagged tracer approach, were analyzed. Surface ozone at the six GAW stations predominantly originated from the NHTS and TRTS in summer and spring. Ozone from the NHTS contributed predominantly to surface ozone in the MMR of China and peaked in summer, with the main sources coming from the region itself. Polluted air masses in MMR were transported by ASM circulations, resulting in high regional background ozone concentrations.

There was a large area surrounding each Chinese GAW station in which the ozone maximum occurred in the same month as it did at the station, confirming the regional representativeness of the surface ozone

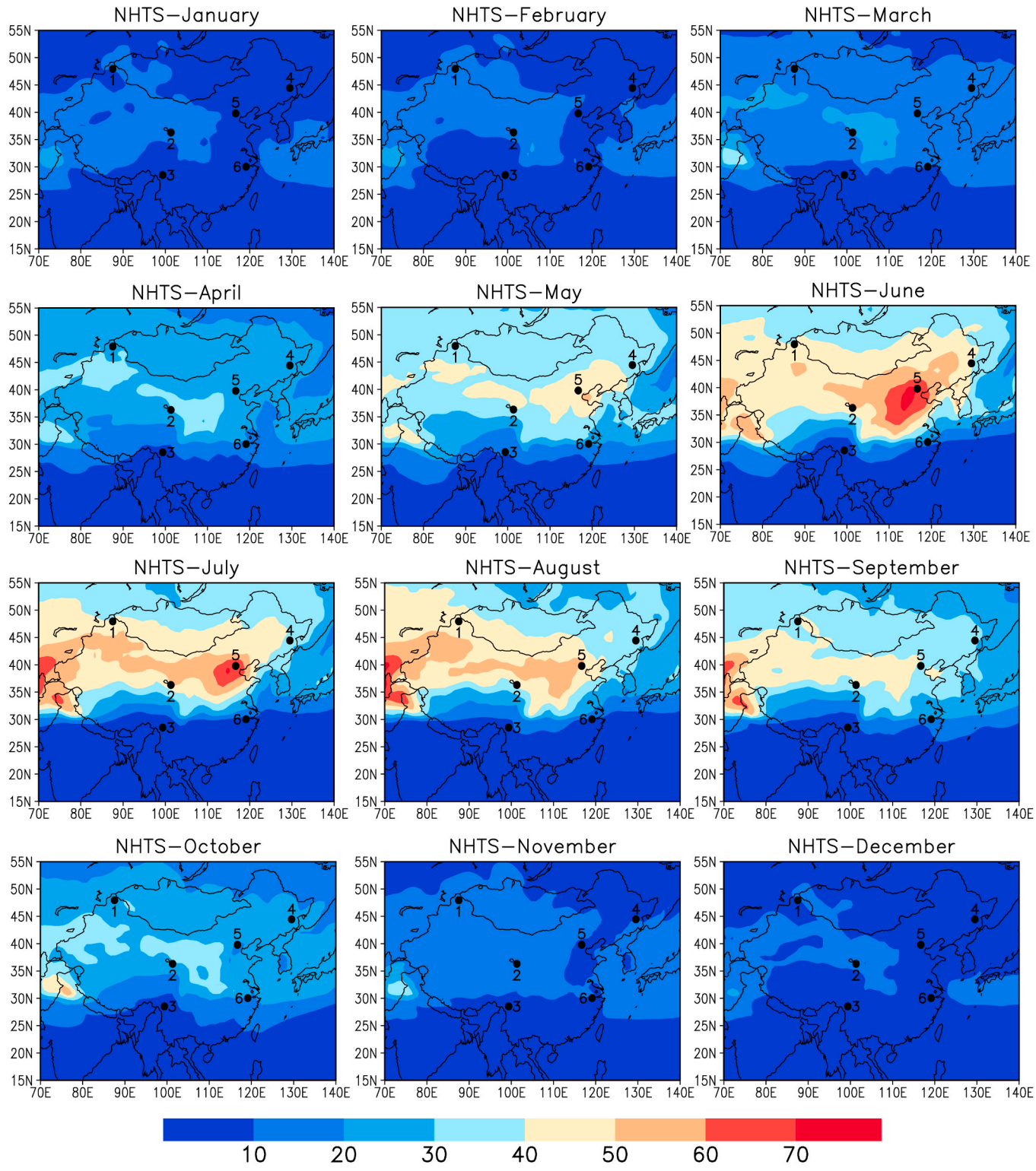

Fig. 7. Simulated regional distributions of the monthly ozone contributions (unit: ppbv) from the NHTS during 2010–2012. Numbers 1 to 6 represent the six GAW stations AKDL, WLG, XGLL, LFS, SDZ, and LN, respectively.

seasonality observed by the Chinese GAW stations. The results will provide a scientific guidance for the construction layout of surface ozone monitoring network in China. In the MMR, the monthly surface ozone maximum occurred consistently in June at SDZ and the whole of the North China Plain, LFS and the Northeast China Plain, and WLG and a northeast-southwest band of the Tibetan Plateau. Tagged ozone from the NHTS also peaked in June and accounted for 90–95%, 91%, and 70–75% of surface ozone concentrations over the three regions, respectively.

In the LMR, the monthly surface ozone maximum at XGLL and the large region to the south of the station occurred in March during the SASM, with ozone from the TRTS peaking in March and accounting for more than 84% of surface ozone concentration over the region. Surface ozone at another LMR station, LN, and the area within 200 km of the station peaked in May at the beginning of the EASM, with ozone from

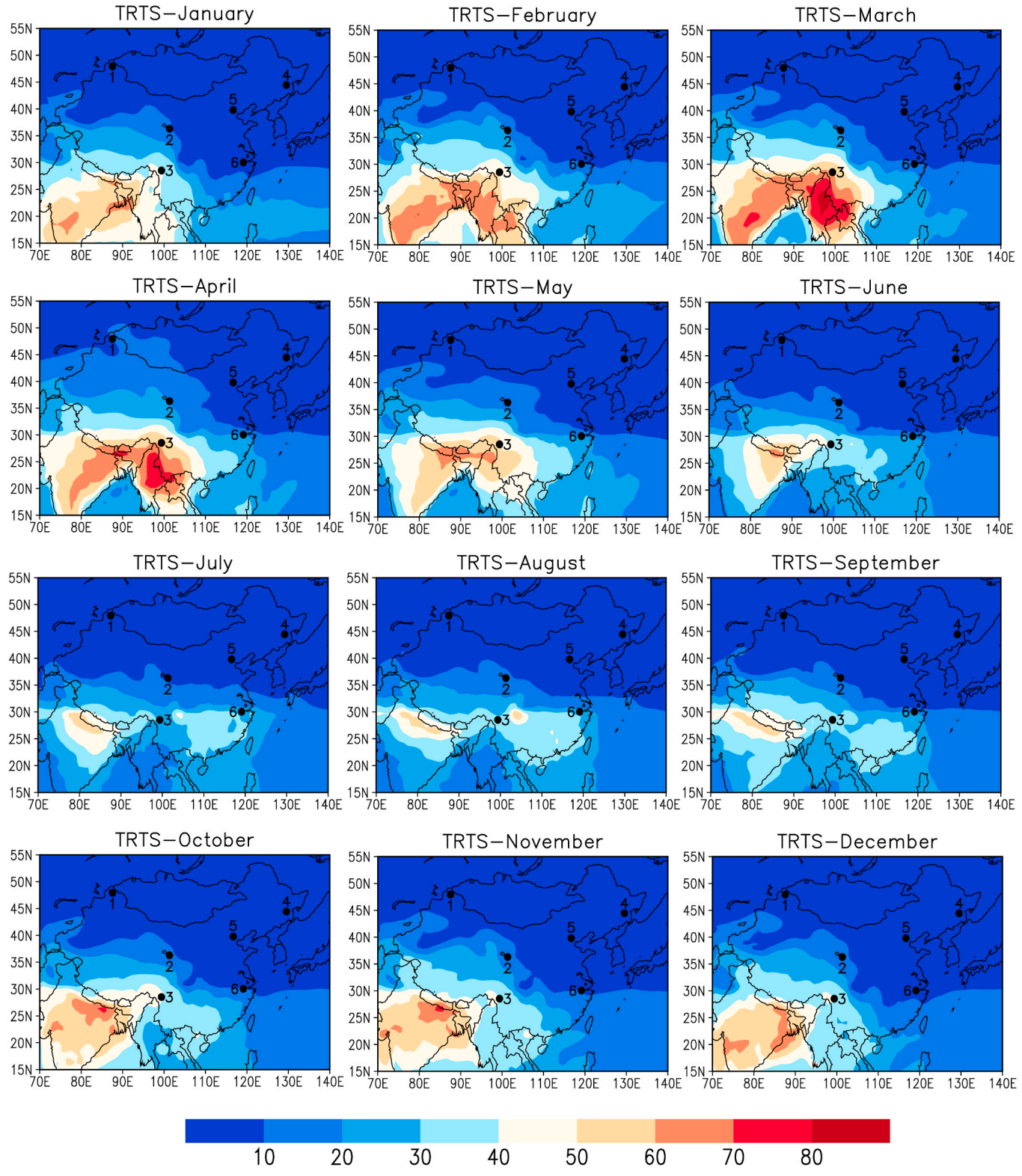

Fig. 8. Same as Fig. 7, but for the TRTS.

the NHTS peaking in May and accounting for approximately 51% of surface ozone concentration over the region, somewhat higher than that of the TRTS (39%) in the same month. The NMR station AKDL and a large region to the south of the station experienced a surface ozone maximum in July. However, in the same month tagged ozone from the NHTS peaked only in a small region to the east and southeast of AKDL, with a contribution above 70%.

In general, surface ozone in China generally peaked in summer over the NMR and MMR, and in spring over the LMR, which shows that the regional representativeness of ozone variation in China is significantly influenced by the ASM.

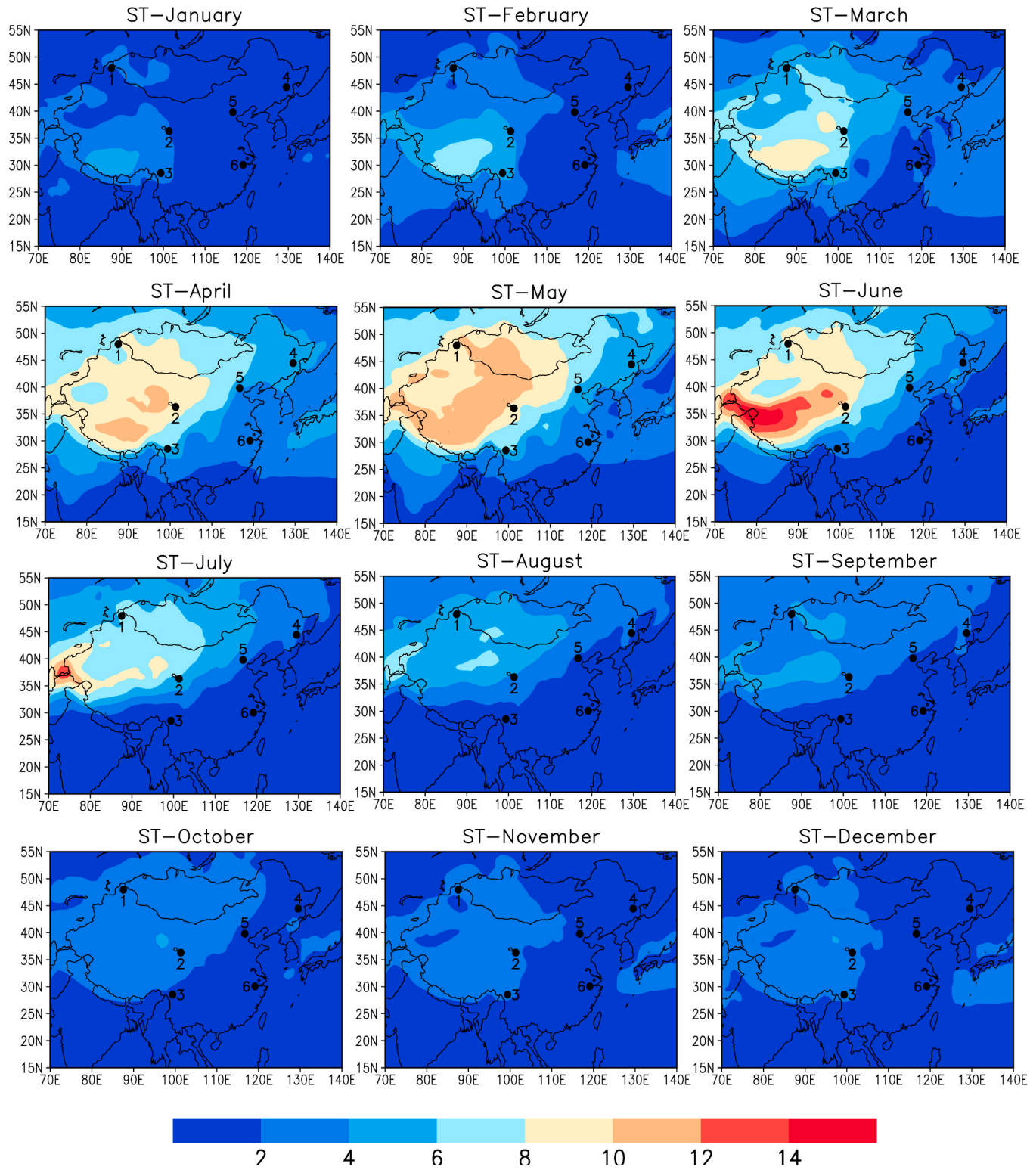

Fig. 9. Same as Fig. 7, but for the ST.

CRediT authorship contribution statement

Ningwei Liu: Methodology, Software, Validation, Formal analysis, Investigation, Writing - original draft, Visualization, Data curation. **Jianzhong Ma:** Conceptualization, Methodology, Software, Writing - review & editing. **Wanyun Xu:** Formal analysis, Writing - review & editing. **Yuhang Wang:** Conceptualization, Writing - review & editing. **Andrea Pozzer:** Methodology, Software. **Jos Lelieveld:** Conceptualization, Writing - review & editing, Supervision.

Declaration of competing interest

The authors declare that they have no known competing financial interests or personal relationships that could have appeared to influence the work reported in this paper.

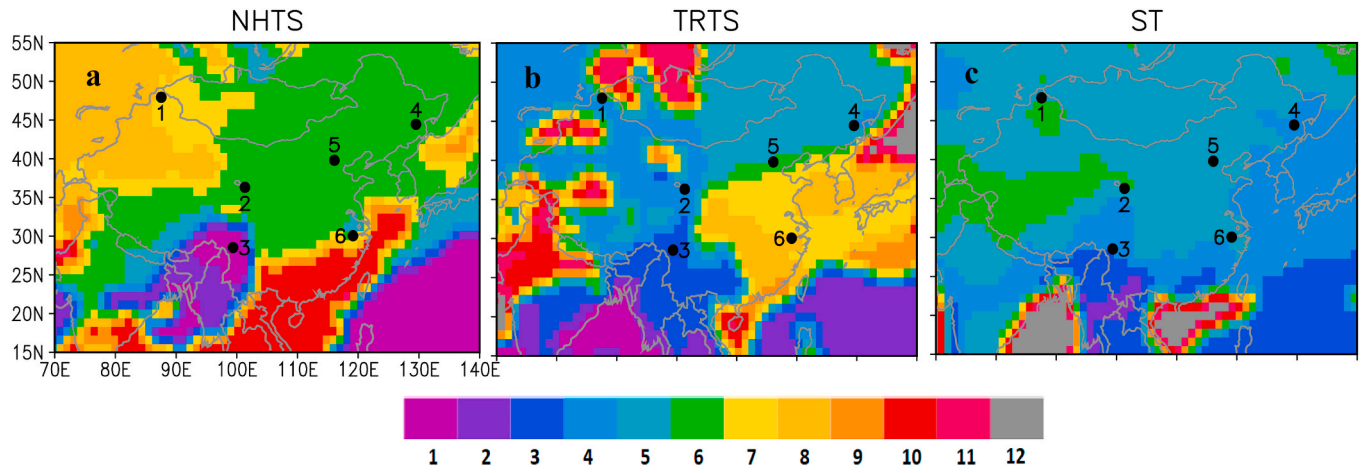

Fig. 10. Regional distributions of the month of occurrence of the maximum surface ozone tracer in each grid in an annual cycle for the NHTS, TRTS, and ST sources, respectively in 2010. Numbers represent the six GAW stations shown in Fig. 1.

Acknowledgements

This work was supported by NSFC under project no. 41875146, the Science & Technology department of Liaoning province under project no. 2019JH8/10300095 and the LAC/CMA under no. 2017B02.

Appendix A. Supplementary data

Supplementary data to this article can be found online at https://doi.org/10.1016/j.atmosenv.2020.117672.

References

Bouwman, A.F., Lee, D.S., Asman, W.A.H., Dentener, F.J., Van Der Hoek, K.W., Olivier, J. G.J., 1997. A global high-resolution emission inventory for ammonia. Global Biogeochem. Cycles 11, 561–587.

Brühl, C., Lelieveld, J., Crutzen, P., Tost, H., 2012. The role of carbonyl sulphide as a source of stratospheric sulphate aerosol and its impact on climate. Atmos. Chem. Phys. 12, 1239–1253.

China Meteorological Bureau, 2015. China Climate Bulletin.

Ding, A., Wang, T., 2006. Influence of stratosphere-to-troposphere exchange on the seasonal cycle of surface ozone at Mount Waliguan in western China. Geophys. Res. Lett. 33.

Grewe, V., 2006. The origin of ozone. Atmos. Chem. Phys. 6, 1495–1511.

He, J., Guo, P., Yin, Y., 2012. Introduction to Atmospheric Science. China Meteorological Press, Beijing.

He, Y., Uno, I., Wang, Z., Pochanart, P., Li, J., Akimoto, H., 2008. Significant impact of the East Asia monsoon on ozone seasonal behavior in the boundary layer of Eastern China and the west Pacific region. Atmos. Chem. Phys. 8, 7543–7555.

Heck, W.W., Taylor, O., Adams, R., Bingham, G., Miller, J., Preston, E., Weinstein, L., 1982. Assessment of crop loss from ozone. J. Air Pollut. Contr. Assoc. 32, 353–361.

Hsu, J., Prather, M.J., 2009. Stratospheric variability and tropospheric ozone. J. Geophys. Res.: Atmosphere 114.

Htap, A.P.S., 2010. Hemispheric Transport of Air Pollution.

Ipcc, A., 2007. Intergovernmental Panel on Climate Change. IPCC Secretariat Geneva.

Jacob, D.J., Logan, J.A., Murti, P.P., 1999. Effect of Rising Asian Emissions on Surface Ozone in the United States.

Jaffe, D., Anderson, T., Covert, D., Kotchenruther, R., Trost, B., Danielson, J., Simpson, W., Berntsen, T., Karlsdottir, S., Blake, D., 1999. Transport of asian air pollution to north America. Geophys. Res. Lett. 26, 711–714.

Jöckel, P., Sander, R., Kerkweg, A., Tost, H., Lelieveld, J., 2005. The modular Earth submodel system (MESSy): a new approach towards Earth system modeling. Atmos. Chem. Phys. 5, 433–444.

Jöckel, P., Tost, H., Pozzer, A., Brühl, C., Buchholz, J., Ganzeveld, L., Hoor, P., Kerkweg, A., Lawrence, M., Sander, R., 2006. The atmospheric chemistry general circulation model ECHAM5/MESSy1: consistent simulation of ozone from the surface to the mesosphere. Atmos. Chem. Phys. Discuss. 6, 6957–7050.

Jöckel, P., Tost, H., Pozzer, A., Kunze, M., Kirner, O., Brenninkmeijer, C., Brinkop, S., Cai, D., Dyroff, C., Eckstein, J., 2016. Earth system chemistry integrated modelling (ESCiMo) with the modular Earth submodel system (MESSy) version 2.51, geosci. Model Dev 9, 1153–1200 gmd-9–1153–2016.

Kerkweg, A., Sander, R., Tost, H., Jöckel, P., Lelieveld, J., 2007. Technical Note: simulation of detailed aerosol chemistry on the global scale using MECCA-AERO. Atmos. Chem. Phys. 7, 2973–2985.

Kirner, O., Ruhnke, R., Buchholz-Dietsch, J., Jöckel, P., Brühl, C., Steil, B., 2010. Simulation of polar stratospheric clouds in the chemistry-climate-model EMAC via the submodel PSC. Geosci. Model Dev. Discuss. (GMDD) 3, 2071–2108.

Lee, D.S., Holland, M.R., Falla, N., 1996. The potential impact of ozone on materials in the UK. Atmos. Environ. 30, 1053–1065.

Lelieveld, J., Dentener, F.J., 2000. What controls tropospheric ozone? J. Geophys. Res. 105, 3531–3551.

Lelieveld, J., Brühl, C., Jöckel, P., Steil, B., Crutzen, P., Fischer, H., Giorgetta, M., Hoor, P., Lawrence, M., Sausen, R., 2007. Stratospheric dryness: model simulations and satellite observations. Atmos. Chem. Phys. 7, 1313–1332.

Levy, H., 1971. Normal atmosphere: large radical and formaldehyde concentrations predicted. Science 173, 141–143.

Lewis, A., Evans, M., Methven, J., Watson, N., Lee, J., Hopkins, J., Purvis, R., Arnold, S., McQuaid, J., Whalley, L., 2007. Chemical composition observed over the mid-Atlantic and the detection of pollution signatures far from source regions. J. Geophys. Res.: Atmosphere 112.

Li, J., Wang, Z., Akimoto, H., Tang, J., Uno, I., 2009. Modeling of the impacts of China's anthropogenic pollutants on the surface ozone summer maximum on the northern Tibetan Plateau. Geophys. Res. Lett. 36.

Li, X., Liu, J., Mauzerall, D.L., Emmons, L.K., Walters, S., Horowitz, L.W., Tao, S., 2014. Effects of trans-Eurasian transport of air pollutants on surface ozone concentrations over Western China. J. Geophys. Res.: Atmosphere 119.

Lin, W., Xu, X., Wang, L., Yang, S., Lin, Y., Zhao, Z., Li, J., Chen, Q., 2010. On-line measurement of reactive gases at Akedala regional atmosphere background station. Meterol. Sci. Technol. 38, 661–667.

Lin, W., Xu, X., Zhang, X., Tang, J., 2008. Contributions of pollutants from North China plain to surface ozone at the Shangdianzi GAW station. Atmos. Chem. Phys. 8, 5889–5898.

Liu, N., Lin, W., Ma, J., Xu, W., Xu, X., 2019. Seasonal variation in surface ozone and its regional characteristics at global atmosphere watch stations in China. J. Environ. Sci. 77, 291–302.

Liu, N., Ma, J., 2017. Seasonal relationships of tropospheric ozone and its precursors over East Asia. J. Appl. Meteorol. Sci. 28, 427–435.

Liu, X., Chance, K., Sioris, C.E., Kurosu, T.P., Spurr, R.J.D., Martin, R.V., Fu, T.M., Logan, J.A., Jacob, D.J., Palmer, P.I., Newchurch, M.J., Megretskaia, I.A., Chatfield, R.B., 2006. First Directly Retrieved Global Distribution of Tropospheric Column Ozone from GOME: Comparison with the GEOS-Chem Model, vol. 111.

Liu, Y., Wang, Y., Liu, X., Cai, Z., Chance, K., 2009. Tibetan middle tropospheric ozone minimum in June discovered from GOME observations. Geophys. Res. Lett. 36.

Ma, J., Brühl, C., He, Q., Steil, B., Karydis, V.A., Klingmüller, K., Tost, H., Chen, B., Jin, Y., Liu, N., Xu, X., Yan, P., Zhou, X., Abdelrahman, K., Pozzer, A., Lelieveld, J., 2019. Modeling the aerosol chemical composition of the tropopause over the Tibetan Plateau during the Asian summer monsoon. Atmos. Chem. Phys. 19, 11587–11612.

Ma, J., Lin, W., Zheng, X., Xu, X., Li, Z., Yang, L., 2014. Influence of air mass downward transport on the variability of surface ozone at Xianggelila Regional Atmosphere Background Station, southwest China. Atmos. Chem. Phys. 14, 5311–5325.

Ma, J., Liu, H., Hauglustaine, D., 2002a. Summertime tropospheric ozone over China simulated with a regional chemical transport model 1. Model description and evaluation. J. Geophys. Res.: Atmosphere 107.

Ma, J., Tang, J., Zhou, X., Zhang, X., 2002b. Estimates of the chemical budget for ozone at Waliguan Observatory. J. Atmos. Chem. 41, 21–48.

Ma, J., Zheng, X., Xu, X., 2005. Comment on "Why does surface ozone peak in summertime at Waliguan?" by Bin Zhu *et al.* Geophys. Res. Lett. 32.

Ma, J., Zhou, X., Hauglustaine, D., 2002c. Summertime tropospheric ozone over China simulated with a regional chemical transport model 2. Source contributions and budget. J. Geophys. Res.: Atmosphere 107.

Ma, Z., Xu, J., Quan, W., Zhang, Z., Lin, W., Xu, X., 2016. Significant increase of surface ozone at a rural site, north of eastern China. Atmos. Chem. Phys. 16, 3969–3977.

Monks, P., Granier, C., Fuzzi, S., Stohl, A., Williams, M., Akimoto, H., Amann, M., Baklanov, A., Baltensperger, U., Bey, I., 2009. Atmospheric composition change–global and regional air quality. Atmos. Environ. 43, 5268–5350.
Pozzer, A., Jöckel, P., Van Aardenne, J., 2009. The influence of the vertical distribution of emissions on tropospheric chemistry. Atmos. Chem. Phys. 9, 9417–9432.
Pozzer, A., Zimmermann, P., Doering, U., Van Aardenne, J., Tost, H., Dentener, F., Janssens-Maenhout, G., Lelieveld, J., 2012. Effects of business-as-usual anthropogenic emissions on air quality. Atmos. Chem. Phys. 12, 6915–6937.
Pringle, K., Tost, H., Steil, B., Giannadaki, D., Nenes, A., Fountoukis, C., Stier, P., Vignati, E., Lelieveld, J., 2010. Description and evaluation of GMXe: a new aerosol submodel for global simulations (v1). Geosci. Model Dev. (GMD) 3, 391.
Safieddine, S., Boynard, A., Hao, N., Huang, F., Wang, L., Ji, D., Barret, B., Ghude, S.D., Coheur, P.-F., Hurtmans, D., 2016. Tropospheric ozone variability during the East Asian summer monsoon as observed by satellite (IASI), aircraft (MOZAIC) and ground stations. Atmos. Chem. Phys. 16, 10489–10500.
Sander, R., Kerkweg, A., Jöckel, P., Lelieveld, J., 2005. Technical note: the new comprehensive atmospheric chemistry module MECCA. Atmos. Chem. Phys. 5, 445–450.
Shindell, D., Kuylenstierna, J.C., Vignati, E., van Dingenen, R., Amann, M., Klimont, Z., Anenberg, S.C., Muller, N., Janssens-Maenhout, G., Raes, F., 2012. Simultaneously mitigating near-term climate change and improving human health and food security. Science 335, 183–189.
Stohl, A., 2004. Intercontinental Transport of Air Pollution. Springer Science & Business Media.
Sun, L., Xue, L., Wang, T., Gao, J., Ding, A., Cooper, O.R., Lin, M., Xu, P., Wang, Z., Wang, X., 2016. Significant increase of summertime ozone at mount tai in central eastern China. Atmos. Chem. Phys. 16, 10637–10650.
Tang, H., Liu, G., Zhu, J., Han, Y., Kobayashi, K., 2013. Seasonal variations in surface ozone as influenced by Asian summer monsoon and biomass burning in agricultural fields of the northern Yangtze River Delta. Atmos. Res. 122, 67–76.
Tost, H., Jöckel, P., Lelieveld, J., 2006. Influence of different convection parameterisations in a GCM. Atmos. Chem. Phys. 6, 5475–5493.
Tost, H., Pringle, K., 2012. Improvements of organic aerosol representations and their effects in large-scale atmospheric models. Atmos. Chem. Phys. 12, 8687.
Wang, H., Jacob, D.J., Le Sager, P., Streets, D.G., Park, R.J., Gilliland, A.B., Van Donkelaar, 2009. Surface ozone background in the United States: Canadian and Mexican pollution influences, 43, 1310–1319.
Wang, T., Cheung, V.T., Anson, M., Li, Y., 2001. Ozone and related gaseous pollutants in the boundary layer of eastern China: overview of the recent measurements at a rural site. Geophys. Res. Lett. 28, 2373–2376.
Wang, T., Ding, A., Gao, J., Wu, W.S., 2006. Strong ozone production in urban plumes from Beijing, China. Geophys. Res. Lett. 33.
Wang, Y., Jacob, D.J., Logan, J.A., 1998. Global simulation of tropospheric O_3-NO^-hydrocarbon chemistry 3. Orig. Trop. Ozone Eff. Nonmethane Hydrocarb. 103 (10), 757-710,767.
Wang, Y., Zhang, Y., Hao, J., Luo, M., 2011. Seasonal and spatial variability of surface ozone over China: contributions from background and domestic pollution. Atmos. Chem. Phys. 11, 3511–3525.
Weinstock, B., Niki, H., 1972. Carbon monoxide balance in nature. Science 176, 290–292.
Wild, O., Pochanart, P., Akimoto, H., 2004. Trans-Eurasian transport of ozone and its precursors. J. Geophys. Res.: Atmosphere 109.
Wofsy, S.C., McConnell, J.C., McElroy, M.B., 1972. Atmospheric CH4, CO, and CO2. J. Geophys. Res. 77, 4477–4493.
Xu, J., Ma, J., Zhang, X., Xu, X., Xu, X., Lin, W., Wang, Y., Meng, W., Ma, Z., 2011. Measurements of ozone and its precursors in Beijing during summertime: impact of urban plumes on ozone pollution in downwind rural areas. Atmos. Chem. Phys. 11, 12241–12252.
Xu, W., Lin, W., Xu, X., Tang, J., Huang, J., Wu, H., Zhang, X., 2016. Long-term trends of surface ozone and its influencing factors at the Mt Waliguan GAW station, China–Part 1: overall trends and characteristics. Atmos. Chem. Phys. 16, 6191–6205.
Xu, X., Ding, G., Li, X., Xiang, R., 1998. Variability and related factors of the surface O_3 at Longfengshan. Acta Meteorol. Sin. 56.
Xu, X., Lin, W., Wang, T., Yan, P., Tang, J., Meng, Z., Wang, Y., 2008. Long-term trend of surface ozone at a regional background station in eastern China 1991–2006: enhanced variability. Atmos. Chem. Phys. 8, 2595–2607.
Xu, X., Liu, X., Lin, W., 2009. Impacts of air parcel transport on the concentrations of trace gases at regional bakground stations. J. Appl. Meteorol. Sci. 20, 656–664.
Xue, L., Wang, T., Guo, H., Blake, D., Tang, J., Zhang, X., Saunders, S., Wang, W., 2013. Sources and photochemistry of volatile organic compounds in the remote atmosphere of western China: results from the Mt. Waliguan Observatory. Atmos. Chem. Phys. 13, 8551–8567.
Xue, L., Wang, T., Zhang, J., Zhang, X., Poon, C., Ding, A., Zhou, X., Wu, W., Tang, J., Zhang, Q., 2011. Source of surface ozone and reactive nitrogen speciation at Mount Waliguan in western China: new insights from the 2006 summer study. J. Geophys. Res.: Atmosphere 116.
Yang, Y., Liao, H., Li, J., 2014. Impacts of the East Asian summer monsoon on interannual variations of summertime surface-layer ozone concentrations over China. Atmos. Chem. Phys. 14, 6867–6879.
Yienger, J.J., Levy II, H., 1995. Empirical model of global soil-biogenic NOχ emissions. J. Geophys. Res.: Atmosphere 100, 11447–11464.
Yin, X., Kang, S., Foy, B.d., Cong, Z., Luo, J., Zhang, L., Ma, Y., Zhang, G., Rupakheti, D., Zhang, Q., 2017. Surface ozone at Nam Co in the inland Tibetan Plateau: variation, synthesis comparison and regional representativeness. Atmos. Chem. Phys. 17, 11293–11311.
Zhao, C., Wang, Y., Yang, Q., Fu, R., Cunnold, D., Choi, Y., 2010. Impact of East Asian summer monsoon on the air quality over China: view from space. J. Geophys. Res.: Atmosphere 115.
Zhou, D., Ding, A., Mao, H., Fu, C., Wang, T., Chan, L., Ding, K., Zhang, Y., Liu, J., Lu, A., 2013. Impacts of the East Asian monsoon on lower tropospheric ozone over coastal South China. Environ. Res. Lett. 8, 044011.
Zhu, B., Akimoto, H., Wang, Z., Sudo, K., Tang, J., Uno, I., 2004. Why does surface ozone peak in summertime at Waliguan? Geophys. Res. Lett. 31.
Zhu, Y., Liu, J., Wang, T., Zhuang, B., Han, H., Wang, H., Chang, Y., Ding, K., 2017. The impacts of meteorology on the seasonal and interannual variabilities of ozone transport from North America to East Asia. J. Geophys. Res.: Atmosphere 122.